Ultrasensitive biosensors based on long-range surface plasmon polariton and dielectric waveguide modes

Leiming Wu,[1,†] Jun Guo,[1,†] Hailin Xu,[2] Xiaoyu Dai,[1] and Yuanjiang Xiang[1,*]

[1]*SZU-NUS Collaborative Innovation Center for Optoelectronic Science & Technology, Key Laboratory of Optoelectronic Devices and Systems of Ministry of Education and Guangdong Province, College of Optoelectronic Engineering, Shenzhen University, Shenzhen 518060, China*

[2]*College of Physics and Energy, Shenzhen University, Shenzhen 518060, China*

**Corresponding author: xiangyuanjiang@126.com*

Received August 9, 2016; revised September 23, 2016; accepted September 25, 2016; posted September 28, 2016 (Doc. ID 273520); published October 20, 2016

An ultrasensitive biosensor based on hybrid structure and composed of long-range surface plasmon polariton (LRSPP) and dielectric planar waveguide (PWG) modes is proposed. Both PWG and LRSPP modes have strong resonances to form strong coupling between the two modes, and the two modes can couple to enhance sensitivity of sensors. In the hybrid structure, PWG is composed of cytop–Si–cytop multilayers and the LRSPP configuration is composed of cytop–metal–sensing medium multilayer slabs. The highest imaging sensitivities of 2264 and 3619 RIU^{-1} were realized in the proposed sensors based on Au and Al-monolayer graphene, respectively, which are nearly 1.2 and 1.9 times larger than the 1910 RIU^{-1} sensitivity of the conventional LRSPR sensor (LRSPP sensor). Moreover, it is demonstrated that the PWG-coupled LRSPP biosensor is applicable to the sensing medium, with refractive index in the vicinity of 1.34.

OCIS codes: (120.0280) Remote sensing and sensors; (130.6010) Sensors; (280.0280) Remote sensing and sensors; (280.1415) Biological sensing and sensors; (280.4788) Optical sensing and sensors; (240.6680) Surface plasmons.

http://dx.doi.org/10.1364/PRJ.4.000262

1. INTRODUCTION

Surface plasmon polariton (SPP) is a special physical phenomenon occurring at the interface of metal and dielectric, where electromagnetic waves are coupled to charge excitations. Usually SPPs can be excited via evanescent waves in attenuated total reflection (ATR) configuration, utilizing high-index prisms, where wave vector mismatch between vacuum and SPPs is compensated. Once SPPs are excited in ATR configuration, a reflectance dip always appears in the reflectance-angle/wavelength curve. SPPs are very sensitive to the refractive index of dielectric attached to the metal surface due to strong light–matter interaction. Therefore, even a small refractive index variation of the dielectric can be detected via measuring changes of SPP excitation. Thus SPP, sensors have various important applications in such areas as food safety testing [1,2], environmental monitoring [3,4], medical diagnosis [5,6], and biochemical applications [7], etc. Ciminelli *et al.* have given a detailed description of the types of biosensors or biochemical sensors [8]. Although SPP sensors have been extensively investigated and applied, higher sensitivities are always pursued by researchers. Long-range surface plasmon polariton (LRSPP) is one of the most effective ways to improve the sensitivity of sensors. LRSPP, first reported by Sarid [9], can be excited through ATR in a thin metal film sandwiched by two dielectrics. When the metal film is thin enough and the two dielectrics have similar refractive index, SPP modes on opposing surfaces of metal film can be coupled together, forming the LRSPP. The dielectric constants of the two dielectrics (ε_1, ε_2) should meet the condition $|\varepsilon_1 - \varepsilon_2| \ll \varepsilon_1, \varepsilon_2$ [10], indicating that LRSPP is more sensitive to changes in the environment than SPP. As a result, the LRSPP sensor has a higher precision compared to a conventional SPP sensor [11,12].

Hybrid configurations composed of two different electromagnetic modes have also attracted much attention in recent years [13–15]. Hayashi *et al.* reported a highly sensitive sensor based on waveguide-coupled SPP, and sensitivity of 1500 RIU^{-1} was demonstrated [13]. Dielectric planar waveguide (PWG) is formed by a dielectric core layer with high refractive index and two cladding layers with low refractive index. Both PWG and LRSPP modes can have strong resonances. If these two modes are successfully coupled together, the phenomenon of normal-mode splitting [16] will occur, which means strong coupling between two modes. When the PWG supports a mode with wave vector close to LRSPP, the two modes may couple to enhance sensitivity of sensors additionally. In this paper, to improve the sensitivity, we propose an ultrasensitive biosensor by using the strong coupling of PWG and LRSPP modes, and enhanced sensitivity of 2264 RIU^{-1} is verified. Moreover, it is also demonstrated that the proposed biosensor can use aluminum (Al) film to replace the Au film in the metal layer, which can further improve the sensitivity. We believe that this scheme could find potential applications in chemical examination, medical diagnosis, and biological detection, etc.

2. THEORETICAL MODELS AND NUMERICAL METHODS

The proposed biosensor is shown in Fig. 1. In the configuration, we choose chalcogenide glass (2S2G) as the coupling prism due to its high refractive index (>2). 2S2G

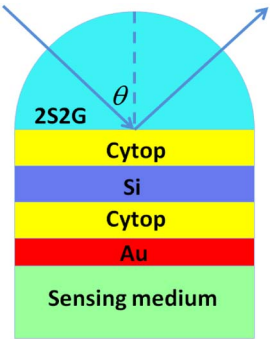

Fig. 1. Schematic diagram of the proposed PWG-coupled LRSPR biosensor based on Au film.

also has shown potential in the fabrication of ultra-low-loss waveguides among glasses [17], and it has been widely used in sensing technology [18–20]. Silicon film with thickness of 14 nm is sandwiched between two cytop layers, and this sandwich structure can work as a PWG. Then PWG is placed under the 2S2G prism. Then a metal film is added, the sensing medium is assumed to be a biomolecule-containing solution with refractive index in the vicinity of 1.34, and the structure of cytop–Au–sensing medium constitutes the LRSPR configuration. Here, the cytop is an amorphous fluoropolymer with a low refractive index that is widely used in LRSPR structures [21,22] and the waveguide structure [13]. Finally, we combine the waveguide structure and LRSPR configuration to obtain a new PWG-coupled LRSPR hybrid structure. The excitation light wavelength is 633 nm, TM-polarized light is incident from the 2S2G glass prism, and the reflective light can be received at the other side through a photon detector.

The first layer is 2S2G prism, and its refractive index is given by the relation $n_1 = 2.24047 + 2.693 \times 10^{-2}/\lambda^2 + 8.08 \times 10^{-3}/\lambda^4$ [18,23], where λ is the wavelength of incident light in micrometers. The dielectrics of the second and fourth layers are cytop films and the refractive index (n_c) is 1.34 at $\lambda =$ 633 nm [21]. The third layer is Si film and its refractive index (n_2) is calculated from the relation $n_2 = A + A_1 e^{-\lambda/t_1} + A_2 e^{-\lambda/t_2}$ [24,25], where $A = 3.44904$, $A_1 = 2271.88813$, $A_2 = 3.39538$, $t_1 = 0.058304$, and $t_2 = 0.30384$. The fifth layer is Al thin film and its dielectric constant follows the Drude–Lorentz model [26], $\varepsilon_m = 1 - \lambda^2\lambda_c/\lambda_p^2(\lambda_c + i\lambda)$, where λ_c and λ_p are the collision and plasma wavelengths, respectively. $\lambda_c = 8.9342 \times 10^{-6}$ m and $\lambda_p = 1.6826 \times 10^{-7}$ m for Au film [27].

In the proposed biosensor, all layers are stacked along the direction perpendicular to the prism, and each layer is defined by the thickness (d_k), refractive index (n_k), and dielectric constant (ε_k), respectively. Therefore, we employ the transfer matrix method [28,29] to analyze the reflectance ($\boldsymbol{R_p}$) of the incident TM-polarized light, and hence the sensitivity is defined as $S = dR_p/dn_s$ [25].

3. NUMERICAL RESULTS AND DISCUSSION

The SPPs at two surfaces of a metal layer can couple together when the metal thickness is small enough. The new coupled modes can be divided into two modes called LRSPPs and short-range surface plasmon polaritons (SRSPPs), according to whether the electric field distribution is asymmetric or not. The dispersion relation should be calculated to decide wave vectors, which are related to incident angle of light directly, of LRSPs and SRSPs; one can refer to the report by Giannini [30].

The dispersion relation for LRSPs is calculated from the formula $\tanh[\alpha d/2] = -\varepsilon_m\alpha_d/\varepsilon_d\alpha$, where ε_m and ε_d are the dielectric constants of metal film and the surrounding dielectric (in the proposed configuration, the surrounding dielectric is cytop), $\alpha_d = \beta^2 - k_0^2\varepsilon_d$, and $\alpha = \beta^2 - k_0^2\varepsilon_m$, where k_0 is the wave vector in vacuum and β is the propagation constant. Hence, the effective index can be defined as $n_{\text{eff}} = \beta/k_0$. Figure 2(a) has shown the effective indices of the LRSPP and PWG modes. First, we calculate that the effective index is 1.3448 (the corresponding incident angle is 34.7721°) for the structure of cytop–Si–cytop when the thickness of Si is 14 nm (solid blue line). Then we can plot the variation of effective indices with respect to the thickness of metal layer for the configuration of cytop–Au–cytop (solid red line). From the figure, we can see that when the thickness of Au is 11.38 nm (this precise thickness is mainly for numerical illustration, while practical thickness need not be so precise), the solid red and blue curves intersect at one point and this means the LRSPP modes can couple with the PWG mode. Figure 3(b) shows the variation of reflectance with respect to the incident angle for the configuration of LRSPR (blue curve) and PWG-coupled LRSPR (red curve) when the thickness of cytop is 2080 nm (note that the outermost cytop layer, which should be replaced by sensing media in practice, is a semi-infinite dielectric). It is obvious that the reflectance curve splits into two dips to obtain two resonance angles (34.7337° and 34.7928°), and both resonance angles are deviated from prediction of individual LRSPP or PWG dispersion indicated by solid lines in Fig. 2(a); this phenomenon is usually called normal-mode coupling or splitting [17]. When normal-mode coupling happens, we can always trace the new dispersion relation by measuring resonance angles numerically. The reflectance curve has two different resonance angles with a fixed thickness of Au film. Assuming that the thickness of Au film is variable, we will get a series of resonance angles and then we can plot the anti-crossing curve (upper branch and lower branch), which is a feature of normal-mode coupling, as the red dotted

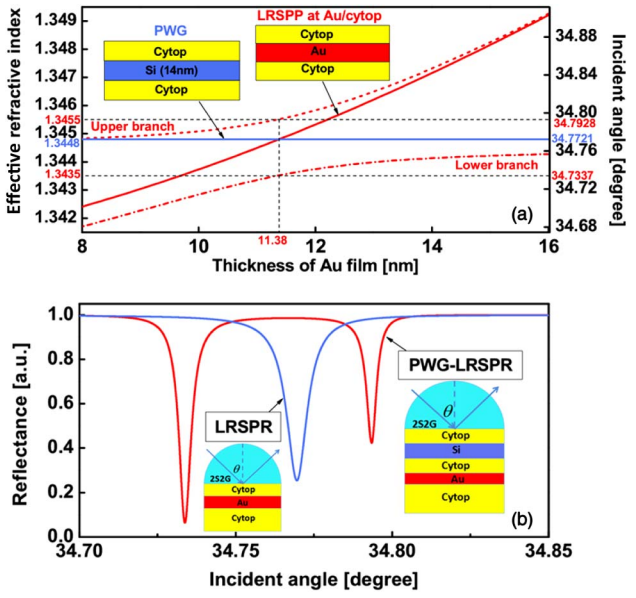

Fig. 2. (a) Effective refractive indices of LRSPP and PWG modes; (b) variation of reflectance with respect to the incident angle for the LRSPR and PWG-coupled LRSPR configurations.

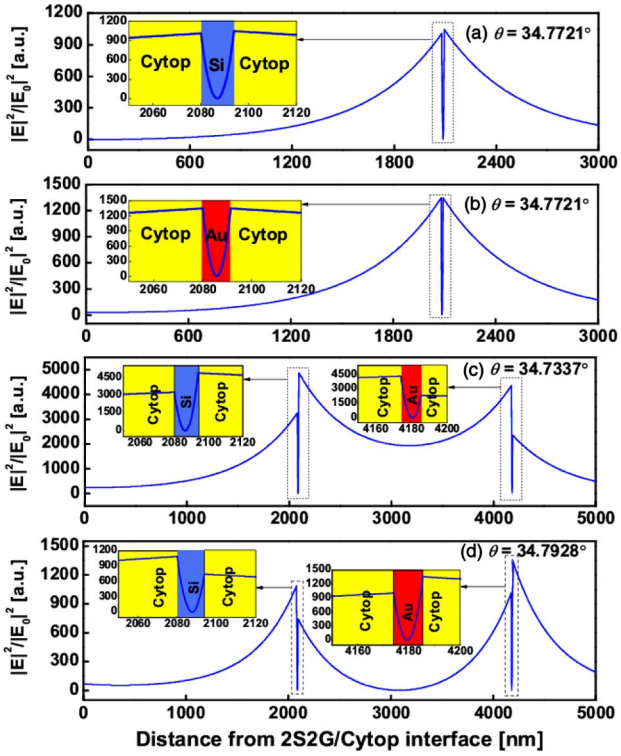

Fig. 3. Schematic diagram of the electric field distributions for the configuration of single (a) PWG and (b) LRSPR; electric field distributions at (c) $\theta = 34.7337°$ and (d) $\theta = 34.7928°$ when the PWG is coupled with LRSPR.

lines shown in Fig. 2(a). From Fig. 2(b), instantly we notice that both the split resonant dips are narrower than the sole dip of LRSPP, which qualitatively indicates higher sensitivity.

We have plotted Fig. 3 to show the tangential electric field distributions for the configuration of PWG and LRSPR at $\theta = 34.7721°$. The field distribution in Figs. 3(a) and 3(b) has the typical features of TM_0 PWG mode and LRSPP. When the PWG mode was coupled with LRSPP mode, the reflectance curve split into two dips. Figures 3(c) and 3(d) are the electric field distributions at $\theta = 34.7337°$ and $\theta = 34.7928°$ (two separate resonance angles), and we can see that the electric field has an obvious improvement at the interface of both cytop/Si and cytop/Au when $\theta = 34.7337°$. Comparing Figs. 3(c) with 3(d), it is clear that the electric field at the interface of cytop/Au for the PWG-coupled LRSPR structure is stronger than the LRSPR structure, which means a stronger coupling between light and electrons at the interface of Au and dielectric. Thus, we can expect that the hybrid structure will be more sensitive to variation of dielectric environment. Hereafter, we replace the last cytop layer with sensing medium to obtain the PWG-coupled LRSPR sensor as shown in Fig. 1. To make sure that the configuration of waveguide can couple with the configuration of LRSPP, the refractive index of the sensing layer is better in the vicinity of 1.34, which may be the refractive index of impure water. We stress that the chosen value of 1.34 is for symmetry and convenience; 1.33 (refractive index of pure water) is also possible, but all figures just discussed should be recalculated. In the proposed imaging sensor, the thickness of cytop is found to be an important factor affecting the sensitivity. To obtain the highest sensitivity, we plot Fig. 4 to determine the optimal

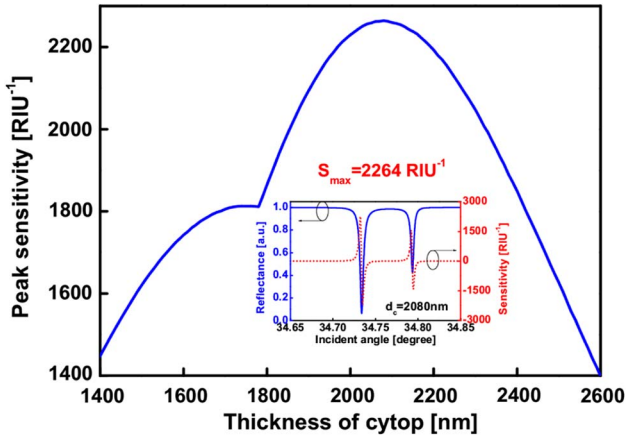

Fig. 4. Variation of peak sensitivity with respect to the thickness of cytop layer for the proposed sensor.

thickness of cytop, and the result shows that sensitivity as high as $2264\,\mathrm{RIU}^{-1}$ can be obtained when the thickness of cytop is 2080 nm. Note that the peak sensitivity may refer to different dips of reflectance, and $S_{\max}$ here is obtained by the left dip. During our calculation, the sensitivity of the waveguide-coupled SRSPP sensor is much lower than that of LRSPP. Therefore, in this paper, we only consider sensors based on PWG-coupled LRSPP. Using the transfer matrix method, we have obtained the reflectance and sensitivity curves for the proposed sensor with optimal thickness. In Fig. 5, we compared sensors based on PWG-coupled LRSPR, LRSPR, and SPR. The results show that the full width at half maximum (FWHM) for the PWG-coupled LRSPR sensor is narrower than the sensors based on LRSPR and SPR, and higher sensitivity can be expected. Here, we calculate the sensitivity by examining changes in the reflectance at a fixed incident angle caused by changes in the refractive

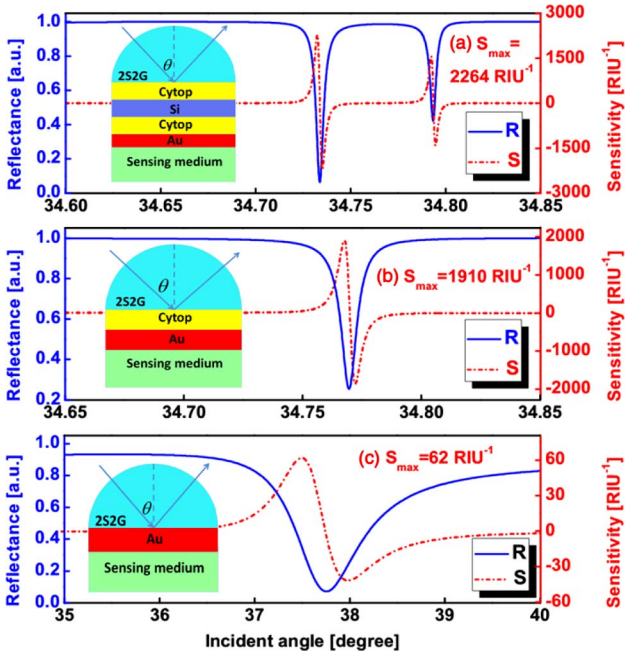

Fig. 5. Variation of reflectance and sensitivity with the incident angle for the sensors based on (a) PWG-coupled LRSPR, (b) LRSPR, and (c) conventional SPR when $n_s = 1.34$.

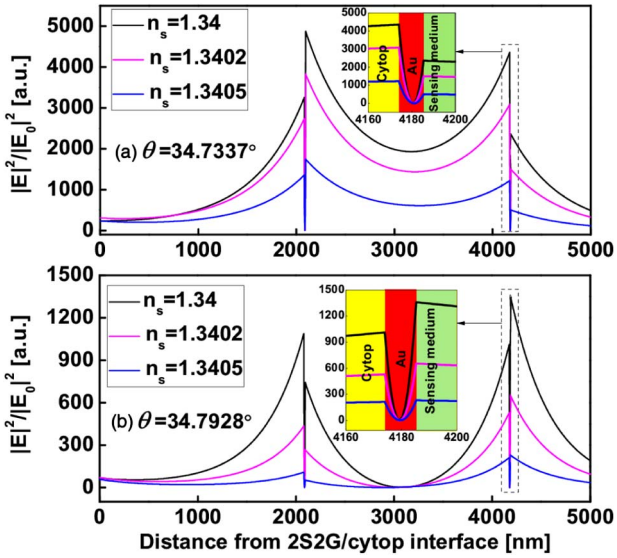

Fig. 6. Schematic diagram of the electric field distributions for the proposed PWG-coupled LRSPR sensor at $\theta = 34.7337°$ and $\theta = 34.7928°$.

index of sensing medium (n_s). For a reflectance dip with narrower FWHM, we can get larger changes in reflectance with a fixed change in n_s, where usually a small change of n_s only shifts the angle of resonance and influences resonance width little. Therefore, a narrower reflectance dip can usually be considered to produce higher sensitivity. It is shown that the reflectance curve in Fig. 5(a) has two dips and it has the highest sensitivity at the first dip. The sensitivities for sensors based on PWG-coupled LRSPR, LRSPR, and SPR are 2264, 1910, and 62 RIU^{-1}, respectively.

In order to understand further the mechanism of the high sensitivity in the proposed sensor, the tangential electric field distributions for different n_s have been shown in Fig. 6. The electric field at the interface of Au/sensing medium will have a dramatic change when n_s has a slight variation. This means that the proposed sensor is very sensitive to the change in sensing medium. We have plotted the variation of peak sensitivity with respect to the change in n_s in the vicinity of 1.34, as shown in Fig. 7. The peak sensitivity increases to its highest value when n_s is near 1.34, and then decreases.

As we know, Au is not susceptible to oxidation and does not react with most chemicals [31,32]; hence, it is often used as

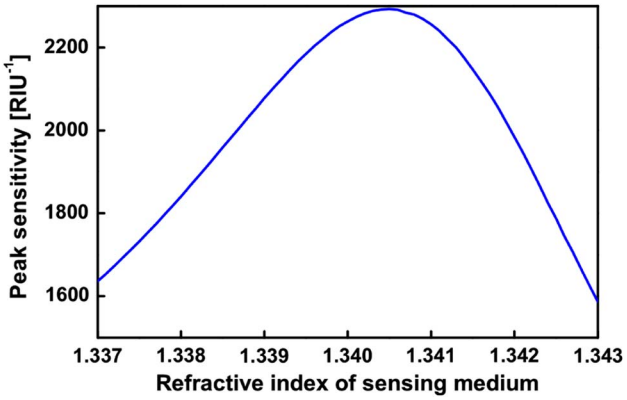

Fig. 7. Variation of peak sensitivity with respect to refractive index of sensing medium in the vicinity of 1.34.

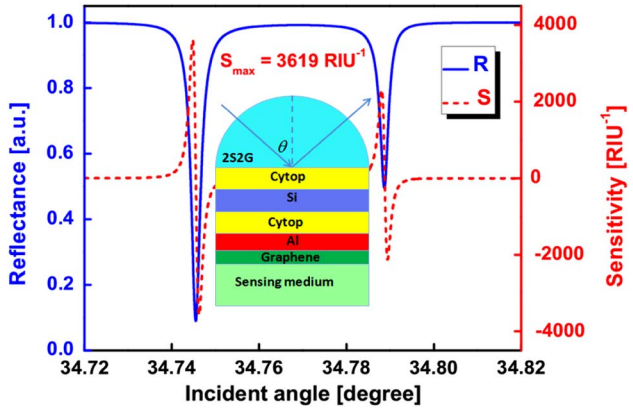

Fig. 8. Variation of reflectance and sensitivity with respect to the incident angle when the thicknesses of cytop and Al are 2350 and 12.4 nm.

the metal film in the sensor. In practical applications, the Au film can be replaced by other metals such as Al, which has been found to have higher sensitivity than Au and silver (Ag) in the application of biosensors [24]. However, Al has poor resistance to oxidation in different environments. In order to prevent Al from oxidizing and increase the biomolecules' adsorption, we introduce graphene. In recent years, the application of graphene has been investigated in various areas such as energy technology [33], hyperbolic metamaterials [34], optical bistability [35,36], and bioassays [37], etc. Especially in optical sensors, graphene has been extensively studied due to its high surface to volume ratio [38] and tunable biocompatibility [39]. Graphene can also be used as the protective layer [24,40] adjoining the biomolecular recognition elements [28] to prevent oxidation and increase the biomolecules' adsorption. More importantly, owing to the ability of graphene to support the electromagnetic waves coupled to charge carriers, combining graphene with metal film to enhance SPP has also attracted considerable attention [41]. Therefore, we can use the structure of Al–graphene to replace the Au film in the proposed sensor to obtain a new biosensor. The thickness of graphene is taken as $d_G = L \times 0.34$ nm (where L is the number of graphene layers), and the refractive index in the visible range is $n_G = 3.0 + iC_1\lambda/3$ [42]. The variation of reflectance and sensitivity with respect to the incident angle is shown in Fig. 8, and the highest sensitivity is 3619 RIU^{-1}. Compared with the Au-based sensor, the sensitivity can have a huge improvement.

4. CONCLUSIONS

In this study, we have proved that the LRSPP mode can couple with PWG mode to obtain an ultrasensitive biosensor. The highest sensitivities for the proposed biosensors based on Au film and Al–graphene are 2246 and 3619 RIU^{-1}, respectively, nearly 1.2 and 1.9 times greater than the sensitivity of LRSPR sensors based on Au film (1910 RIU^{-1}) and nearly 36 and 58 times greater than the sensitivity of conventional SPR sensors (62 RIU^{-1}). The present biosensor has shown a strong SPR excitation and a high sensitivity to analyte, and the biosensor is applicable to the sensing medium, with refractive index in vicinity of 1.34. With such an excellent performance, we believe that this novel structure can play an active role in the field of optical sensing technology.

Funding. National Natural Science Foundation of China (NSFC) (61505111); Guandong Natural Science Foundation (2015A030313549); Science and Technology Planning Project of Guangdong Province (2016B050501005); Science and Technology Project of Shenzhen (JCYJ20140828163633996, JCYJ20150324141711667); Natural Science Foundation of SZU (201452, 201517, 827-000051, 827-000052, 827-000059).

†These authors contributed equally.

REFERENCES

1. J. Homola, J. Dostalek, S. Chen, A. Rasooly, S. Jiang, and S. S. Yee, "Spectral surface plasmon resonance biosensor for detection of staphylococcal enterotoxin B in milk," Int. J. Food Microbiol. **75**, 61–69 (2002).
2. A. Rasooly, "Surface plasmon resonance analysis of staphylococcal enterotoxin B in food," J. Food Protect. **64**, 37–43 (2001).
3. E. Mauriz, A. Calle, J. J. Manclús, A. Montoya, and L. M. Lechuga, "Multi-analyte SPR immunoassays for environmental biosensing of pesticides," Anal. Bionanal. Chem. **387**, 1449–1458 (2007).
4. C. Hu, N. Gan, Y. Chen, L. Bi, X. Zhang, and L. Song, "Detection of microcystins in environmental samples using surface plasmon resonance biosensor," Talanta **80**, 407–410 (2009).
5. J. W. Chung, S. D. Kim, R. Bernhardt, and J. C. Pyun, "Application of SPR biosensor for medical diagnostics of human hepatitis B virus (hHBV)," Sens. Actuators B **111**, 416–422 (2005).
6. J. Ladd, A. D. Taylor, M. Piliarik, J. Homola, and S. Jiang, "Label-free detection of cancer biomarker candidates using surface plasmon resonance imaging," Anal. Bioanal. Chem. **393**, 1157–1163 (2009).
7. D. Conteduca, F. Dell'Olio, F. Innone, C. Ciminelli, and M. N. Armenise, "Rigorous design of an ultra-high Q/V photonic/plasmonic cavity to be used in biosensing applications," Opt. Laser Technol. **77**, 151–161 (2016).
8. C. Ciminelli, C. M. Campanella, F. Dell'Olio, C. E. Campanella, and M. N. Armenise, "Label-free optical resonant sensors for biochemical applications," Prog. Quantum Electron. **37**, 51–107 (2013).
9. D. Sarid, "Long-range surface-plasma waves on very thin metal films," Phys. Rev. Lett. **47**, 1927–1930 (1981).
10. F. Yang, J. R. Sambles, and G. W. Bradberry, "Long-range surface modes supported by thin films," Phys. Rev. B **44**, 5855–5872 (1991).
11. K. Matsubara, S. Kawata, and S. Minami, "Multilayer system for a high-precision surface plasmon resonance sensor," Opt. Lett. **15**, 75–77 (1990).
12. J. Dostálek, A. Kasry, and W. Knoll, "Long range surface plasmons for observation of biomolecular binding events at metallic surfaces," Plasmonics **2**, 97–106 (2007).
13. S. Hayashi, D. V. Nesterenko, and Z. Sekkat, "Fano resonance and plasmon-induced transparency in waveguide-coupled surface plasmon resonance sensors," Appl. Phys. Express **8**, 022201 (2015).
14. Z. Salamon, H. A. Macleod, and G. Tollin, "Coupled plasmon-waveguide resonators: a new spectroscopic tool for probing proteolipid film structure and properties," Biophys. J. **73**, 2791–2797 (1997).
15. J. Homola, "Surface plasmon resonance sensors for detection of chemical and biological species," Chem. Rev. **108**, 462–493 (2008).
16. G. Khitrova, H. M. Gibbs, F. Jahnke, M. Kira, and S. W. Koch, "Nonlinear optics of normal-mode-coupling semiconductor microcavities," Rev. Mod. Phys. **71**, 1591–1639 (1999).
17. V. G. Ta'Eed, M. R. E. Lamont, D. J. Moss, B. J. Eggleton, D. Y. Choi, S. Madden, and B. Luther-Davies, "All optical wavelength conversion via cross phase modulation in chalcogenide glass rib waveguides," Opt. Express **14**, 11242–11247 (2006).
18. P. K. Maharana and R. Jha, "Chalcogenide prism and graphene multilayer based surface plasmon resonance affinity biosensor for high performance," Sens. Actuators B **169**, 161–166 (2012).
19. P. K. Maharana, R. Jha, and S. Palei, "Sensitivity enhancement by air mediated graphene multilayer based surface plasmon resonance biosensor for near infrared," Sens. Actuators B **190**, 494–501 (2014).
20. P. K. Maharana, S. Bharadwaj, and R. Jha, "Electric field enhancement in surface plasmon resonance bimetallic configuration based on chalcogenide prism," J. Appl. Phys. **114**, 014304 (2013).
21. A. W. Wark, H. J. Lee, and R. M. Corn, "Long-range surface plasmon resonance imaging for bioaffinity sensors," Anal. Chem. **77**, 3904–3907 (2005).
22. Y. Wang, A. Brunsen, U. Jonas, J. Dostalek, and W. Knoll, "Prostate specific antigen biosensor based on long range surface plasmon-enhanced fluorescence spectroscopy and dextran hydrogel binding matrix," Anal. Chem. **81**, 9625–9632 (2009).
23. R. Jha and A. K. Sharma, "Chalcogenide glass prism based SPR sensor with Ag–Au bimetallic nanoparticle alloy in infrared wavelength region," J. Opt. A **11**, 045502 (2009).
24. P. K. Maharana, T. Srivastava, and R. Jha, "On the performance of highly sensitive and accurate graphene-on-aluminum and silicon-based SPR biosensor for visible and near infrared," Plasmonics **9**, 1113–1120 (2014).
25. R. Verma, B. D. Gupta, and R. Jha, "Sensitivity enhancement of a surface plasmon resonance based biomolecules sensor using graphene and silicon layers," Sens. Actuators B **160**, 623–631 (2011).
26. S. Zeng, S. Hu, J. Xia, A. Tommy, Q. D. Xuan, M. M. Xiang, C. Philippe, and Y. Ken-Tye, "Graphene-MoS_2 hybrid nanostructures enhanced surface plasmon resonance biosensors," Sens. Actuators B **207**, 801–810 (2015).
27. A. K. Sharma and B. D. Gupta, "On the performance of different bimetallic combinations in surface plasmon resonance based fiber optic sensors," J. Appl. Phys. **101**, 093111 (2007).
28. L. Wu, H. S. Chu, W. S. Koh, and E. P. Li, "Highly sensitive graphene biosensors based on surface plasmon resonance," Opt. Express **18**, 14395–14400 (2010).
29. B. D. Gupta and A. K. Sharma, "Sensitivity evaluation of a multilayered surface plasmon resonance-based fiber optic sensor: a theoretical study," Sens. Actuators B **107**, 40–46 (2005).
30. V. Giannini, Y. Zhang, M. Forcales, and J. Gómez Rivas, "Long-range surface polaritons in ultra-thin films of silicon," Opt. Express **16**, 19674–19685 (2008).
31. O. Krupin, H. Asiri, C. Wang, R. N. Tait, and P. Berini, "Biosensing using straight long-range surface plasmon waveguides," Opt. Express **21**, 698–709 (2013).
32. J. C. Love, L. A. Estroff, J. K. Kriebel, R. G. Nuzzo, and G. M. Whitesides, "Self-assembled monolayers of thiolates on metals as a form of nanotechnology," Chem. Rev. **105**, 1103–1170 (2005).
33. N. G. Sahoo, Y. Pan, L. Li, and S. H. Chan, "Graphene-based materials for energy conversion," Adv. Mater. **24**, 4203–4210 (2012).
34. Y. Xiang, X. Dai, J. Guo, H. Zhang, S. Wen, and D. Tang, "Critical coupling with graphene-based hyperbolic metamaterials," Sci. Rep. **4**, 5483 (2014).
35. Y. Xiang, X. Dai, J. Guo, and S. Wen, "Tunable optical bistability at the graphene-covered nonlinear interface," Appl. Phys. Lett. **104**, 051108 (2014).
36. X. Dai, L. Jiang, and Y. Xiang, "Low threshold optical bistability at terahertz frequencies with graphene surface plasmons," Sci. Rep. **5**, 12271 (2015).
37. L. Wu, Z. Ling, L. Jiang, J. Guo, X. Dai, Y. Xiang, and D. Fan, "Long-range surface plasmon with graphene for enhancing the sensitivity and detection accuracy of biosensor," IEEE Photon. J. **8**, 4801409 (2016).
38. Y. Zhu, S. Murali, W. Cai, X. Li, J. W. Suk, J. R. Potts, and R. S. Ruoff, "Graphene and graphene oxide: synthesis, properties, and applications," Adv. Mater. **22**, 3906–3924 (2010).
39. H. Fan, L. Wang, K. Zhao, N. Li, Z. Shi, Z. Ge, and Z. Jin, "Fabrication, mechanical properties, and biocompatibility of graphene-reinforced chitosan composites," Biomacromolecules **11**, 2345–2351 (2010).
40. S. H. Choi, Y. L. Kim, and K. M. Byun, "Graphene-on-silver substrates for sensitive surface plasmon resonance imaging biosensors," Opt. Express **19**, 458–466 (2011).
41. F. H. Koppens, D. E. Chang, and F. J. Garcia de Abajo, "Graphene plasmonics: a platform for strong light-matter interactions," Nano Lett. **11**, 3370–3377 (2011).
42. M. Bruna and S. Borini, "Optical constants of graphene layers in the visible range," Appl. Phys. Lett. **94**, 031901 (2009).